

# Room temperature ferromagnetic semiconductors through metal-semiconductor transition in monolayer MnSe<sub>2</sub>

Jia-Wen Li,<sup>1</sup> Gang Su,<sup>1,2,3,4,\*</sup> and Bo Gu<sup>1,2,3,†</sup>

<sup>1</sup>*Kavli Institute for Theoretical Sciences, University of Chinese Academy of Sciences, Beijing 100049, China*

<sup>2</sup>*CAS Center for Excellence in Topological Quantum Computation,  
University of Chinese Academy of Sciences, Beijing 100190, China*

<sup>3</sup>*Physical Science Laboratory, Huairou National Comprehensive Science Center, Beijing 101400, China*

<sup>4</sup>*School of Physical Sciences, University of Chinese Academy of Sciences, Beijing 100049, China*

To realize room temperature ferromagnetic semiconductors is still a challenge in spintronics. Recent experiments have obtained two-dimensional (2D) room temperature ferromagnetic metals, such as monolayer MnSe<sub>2</sub>. In this paper, we proposed a way to obtain room temperature ferromagnetic semiconductors through metal-semiconductor transition. By the density functional theory calculations, a room temperature ferromagnetic semiconductor is obtained in monolayer MnSe<sub>2</sub> with a few percent tensile strains, where a metal-semiconductor transition occurs with 2.2% tensile strain. The tensile strains raise the energy of d orbitals of Mn atoms and p orbitals of Se atoms near the Fermi level, making the Fermi level sets in the energy gap of bonding and antibonding states of these p and d orbitals, and opening a small band gap. The room temperature ferromagnetic semiconductors are also obtained in the heterostructures MnSe<sub>2</sub>/X (X = Al<sub>2</sub>Se<sub>3</sub>, GaSe, SiH, and GaP), where metal-semiconductor transition happens due to the tensile strains by interface of heterostructures. In addition, a large magneto-optical Kerr effect (MOKE) is obtained in monolayer MnSe<sub>2</sub> with tensile strain and MnSe<sub>2</sub>-based heterostructures. Our theoretical results pave a way to obtain room temperature magnetic semiconductors from experimentally obtained 2D room temperature ferromagnetic metals through metal-semiconductor transitions.

## I. INTRODUCTION

In spintronics, it is still a challenge in experiments to realize room temperature ferromagnetic semiconductors. In 2017, the successful synthesis of two-dimensional (2D) van der Waals ferromagnetic semiconductors CrI<sub>3</sub> [1] and Cr<sub>2</sub>Ge<sub>2</sub>Te<sub>6</sub> [2] in experiments has attracted extensive attention to 2D ferromagnetic semiconductors. According to Mermin-Wagner theorem [3], the magnetic anisotropy is essential to produce long-range magnetic order in 2D systems. Recently, more 2D ferromagnetic semiconductors have been obtained in experiments, such as Cr<sub>2</sub>S<sub>3</sub> [4], CrCl<sub>3</sub> [5], CrBr<sub>3</sub> [6], CrSiTe<sub>3</sub> [7], CrSBr [8], where the Curie temperatures  $T_C$  are far below room temperature. On the other hand, the 2D van der Waals ferromagnetic metals with high  $T_C$  have been obtained in recent experiments. For example,  $T_C = 140$  K in CrTe [9], 300 K in CrTe<sub>2</sub> [10], 344 K in Cr<sub>3</sub>Te<sub>6</sub> [11], 160 K in Cr<sub>3</sub>Te<sub>4</sub> [12], 280 K in CrSe [13], 300 K in Fe<sub>3</sub>GeTe<sub>2</sub> [14, 15], 270 K in Fe<sub>4</sub>GeTe<sub>2</sub> [16], 229 K in Fe<sub>5</sub>GeTe<sub>2</sub> [17], 380 K in Fe<sub>3</sub>GaTe<sub>2</sub> [18], 300 K in MnSe<sub>2</sub> [19], etc.

Recent studies have shown that the physical properties of 2D materials are sensitive to external regulations, such as electric field [14, 20–23], doping [24–28], surface functionalization [29, 30], intercalation [31, 32], heterostructure [33–48], strain [34, 49–53], etc. Among them, strain engineering is an effective technique to change the lattice and electronic structures and thus to control various

properties of 2D materials. In contrast to bulk materials, 2D materials have stronger deformation capacity and thus can withstand greater elastic strain without fracture, which shows great advantages in strain engineering. For example, monolayer MoS<sub>2</sub> can sustain strains as large as 11% [54], monolayer FeSe can sustain strains up to 6% [55, 56], and single-layer graphene can even withstand 25% elastic strain [57]. It has been observed that in few-layer black phosphorus that biaxial tensile strain can increase the band gap, while biaxial compressive strain can decrease the band gap [49]. Under uniaxial strain up to 1.7%, a band gap reduction of 0.3 eV was observed in monolayer MoS<sub>2</sub> [50].

In addition, heterostructures can have a significant impact on the magnetism of magnetic materials [38–40, 45–47]. Heterostructures also have a great impact on the band structure. Especially, due to the effect of interlayer interaction and strain, metal-semiconductor transition happens in some semimetal/semiconductor heterostructures, and a band gap  $E_g$  can be opened, such as  $E_g = 0.44$  eV in silicene/GaP [41], 0.22 eV in silicene/Ga<sub>2</sub>SeS [42], 0.67 eV in CSe/BP [58], 13 meV in graphene/MoSi<sub>2</sub>N<sub>4</sub> [43] and 17 meV in Ge/SMoSe [44].

As a room temperature ferromagnetic material, MnSe<sub>2</sub> has attracted a lot of attentions due to its interesting properties [36, 37, 59–66]. The structure of MnSe<sub>2</sub> is shown in Fig. 1(a) with space group of P $\bar{3}$ m1 (164). The band structure from density functional theory (DFT) with Perdew-Burke-Ernzerhof (PBE) pseudopotential shows semimetal properties [62–65]. Because PBE pseudopotential always underestimated the band gap, Heyd-Scuseria-Ernzerhof (HSE) hybrid functional approach is believed to give a better description of the

\* gsu@ucas.ac.cn

† gubo@ucas.ac.cn

band structures [67]. By the DFT with HSE, MnSe<sub>2</sub> was calculated to be a semimetal [45, 63] or semiconductor with small band gap of 0.01 eV [65]. Experimental results suggest that MnSe<sub>2</sub> at Bi<sub>2</sub>Se<sub>3</sub> substrate has a small band gap [60]. On the other hand, the electronic properties of monolayer MnSe<sub>2</sub> are still unclear. It was reported that tensile strain could enhance the ferromagnetic properties of monolayer MnSe<sub>2</sub> and weaken the metallicity [63, 65]. It has been discussed that  $T_C$  can be enhanced by tensile strain in some 2D ferromagnetic semiconductors [38, 68–70]. The evolution of band structures of monolayer MnSe<sub>2</sub> was calculated by DFT with PBE, giving no band gap with tensile strain up to 8% [65]. Is it possible to open a band gap in these room temperature ferromagnetic metals by some methods, and obtain room temperature ferromagnetic semiconductors?

In this paper, we propose a way to obtain room temperature ferromagnetic semiconductor by metal-semiconductor transition in monolayer MnSe<sub>2</sub> and MnSe<sub>2</sub>-based heterostructures. The DFT calculation with HSE hybrid functional shows that monolayer MnSe<sub>2</sub> is room temperature ferromagnetic semimetal. A 2.2% tensile strain could open a small band gap in monolayer MnSe<sub>2</sub>. An in-plane to out-of-plane magnetic anisotropy transition happens with 1.7% tensile strain, and  $T_C$  increases with tensile strain. In addition, the heterostructures MnSe<sub>2</sub>/X with X= GaP [71–73], GaSe [74], SiH [75], and Al<sub>2</sub>Se<sub>3</sub> [40] were studied. The room temperature ferromagnetic semiconductors are also obtained in these heterostructures, where metal-semiconductor transition occurs due to tensile strain by interfaces. Large magneto-optical Kerr effect is found in monolayer MnSe<sub>2</sub> with a percent tensile strain and MnSe<sub>2</sub>-based heterostructures. Our theoretical results propose a way to obtain room temperature ferromagnetic semiconductors by metal-semiconductor transition in monolayer MnSe<sub>2</sub> by applying tensile strain or building heterostructures.

## II. METHOD

All calculations were based on the DFT as implemented in the Vienna ab initio simulation package (VASP) [76]. The exchange-correlation potential is described by the PBE form with the generalized gradient approximation (GGA) [77]. The electron-ion potential is described by the projector-augmented wave (PAW) method [78]. We carried out the calculation of PBE + U with U = 4 eV for 3d electrons in Mn [62–65]. The band structures were calculated in HSE06 hybrid functional [67]. The plane-wave cutoff energy is set to be 650 eV. The  $9 \times 9 \times 1$   $\Gamma$  center K-point was used for the Brillouin zone (BZ) sampling. To obtain accurate results of magnetic anisotropy energy (MAE), K-points were chosen as  $\Gamma$ -centered  $25 \times 25 \times 1$ . The density of states (DOS) were obtained from HSE and K-points of  $\Gamma$ -centered  $18 \times 18 \times 1$ . The structures of all materials were fully relaxed, where the convergence precision of energy and force was  $10^{-6}$

eV and  $10^{-2}$  eV/Å, respectively. The van der Waals effect is included with DFT-D3 method [79]. The Wannier90 code was used to construct a tight-binding Hamiltonian [80, 81]. The WannierTools code was used to obtain a tight-binding band structure from tight-binding Hamiltonian [82]. The Heisenberg-type Monte Carlo simulation was performed on a  $50 \times 50 \times 1$  lattice with 2500 magnetic points for MnSe<sub>2</sub>.  $1 \times 10^5$  steps were carried for each temperature, and the last one-thirds steps were used to calculate the temperature-dependent physical quantities.

## III. RESULTS AND DISCUSSION

### A. Monolayer MnSe<sub>2</sub>

The crystal structure of monolayer MnSe<sub>2</sub> is shown in Fig. 1(a), which shows a triangle lattice. The calculated in-plane lattice constant is  $a_0 = 3.658$  Å, in agreement with previous calculations [62–65]. The band structure of monolayer MnSe<sub>2</sub> with HSE hybrid functional is shown in Fig. 1(b). The lowest band above Fermi level and the highest band below Fermi level slightly overlap, showing the semimetal behavior. The bands near Fermi level contain only one component of spins, showing the half-metal behavior. In addition, the Monte Carlo results of magnetization and susceptibility as a function of temperature for monolayer MnSe<sub>2</sub> is shown in Fig. 1(c), giving a high  $T_C = 354$  K.

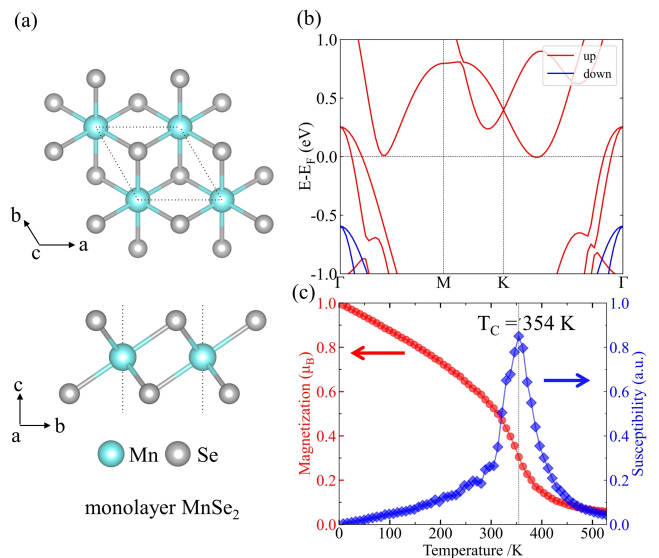


FIG. 1. (a) Top and side views of crystal structure of monolayer MnSe<sub>2</sub>. (b) Spin polarized band structure of MnSe<sub>2</sub>, obtained by the DFT calculation with HSE hybrid functional. (c) Magnetization and susceptibility of MnSe<sub>2</sub> as a function of temperature, obtained by the Monte Carlo simulation based on a 2D Heisenberg model. The Curie temperature of monolayer MnSe<sub>2</sub> is calculated as  $T_C = 354$  K, being consistent with the experiment [19].

## B. Monolayer MnSe<sub>2</sub> with strain

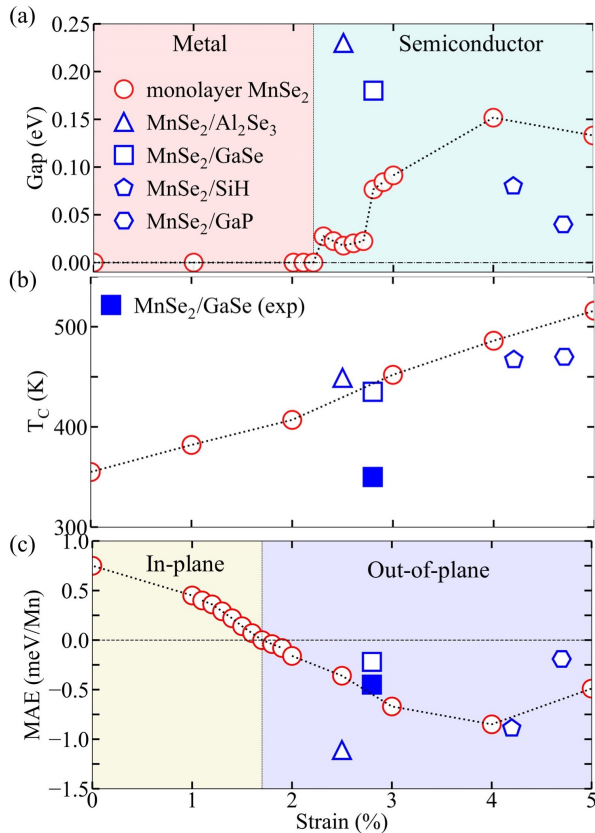


FIG. 2. For monolayer MnSe<sub>2</sub>, tensile strain dependence of (a) band gap, (b) Curie temperature  $T_C$ , and (c) magnetic anisotropy energy (MAE), obtained by the DFT and Monte Carlo calculations. Numerical results of four MnSe<sub>2</sub>-based heterostructures are also included, where strain comes from the interface of heterostructures. Experimental  $T_C$  and MAE of heterostructure MnSe<sub>2</sub>/GaSe [19] are included for comparison.

To study the effect of strain on electronic properties, we applied biaxial strain. The strain ratio is defined as  $\epsilon = (a - a_0)/a_0$ , where  $a$  and  $a_0$  are the in-plane lattice constants with and without strain, respectively. The variation of band gap of monolayer MnSe<sub>2</sub> with tensile strain calculated by DFT with HSE is shown in Fig. 2 (a). A metal-semiconductor transition happens with a tensile strain of 2.2%. Fig. 2 (b) shows  $T_C$  of monolayer MnSe<sub>2</sub> as a function with tensile strain.  $T_C$  increase with tensile strain, in agreement with previous report [38, 68–70]. The MAE is defined as  $(E_{\perp} - E_{\parallel})/N_{Mn}$ , where  $E_{\perp}$  and  $E_{\parallel}$  are energies of MnSe<sub>2</sub> with out-of-plane and in-plane magnetic polarization, respectively.  $N_{Mn}$  is the number of Mn atoms in a unit cell. For monolayer MnSe<sub>2</sub> without strain, as shown in Fig. 2(c), the in-plane MAE of 0.75 meV/Mn is obtained, in agreement with the previous report [63]. By applying tensile strain, an in-plane to out-plane MAE transition is obtained at 1.7% tensile strain. Thus, monolayer MnSe<sub>2</sub> will become a room tem-

perature ferromagnetic semiconductor with out-of-plane MAE by applying tensile strains above 2.2%.

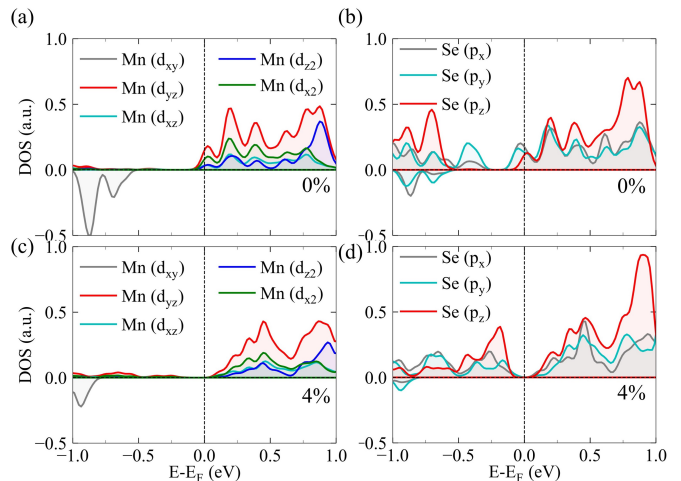


FIG. 3. Metal-semiconductor transition of monolayer MnSe<sub>2</sub> due to strain. DFT results of partial density of state (PDOS) of (a) d orbitals of Mn and (b) p orbitals of Se without strain. PDOS of (c) d orbitals of Mn and (d) p orbitals of Se with 4% tensile strain.

In order to analyze the metal-semiconductor transition of monolayer MnSe<sub>2</sub> under strain, the partial density of states (PDOS) were calculated, as shown in Fig. 3. PDOS of d orbitals of Mn and p orbitals of Se without strain is shown in Figs. 3(a) and 3(b), respectively. PDOS of Mn and Se with 4% tensile strain is shown in Figs. 3(c) and 3(d), respectively, with a small gap. The tensile strains raise the energy of d orbitals of Mn atoms and p orbitals of Se atoms near the Fermi level, making the Fermi level lie in the energy gap of bonding and antibonding states of these p and d orbitals, and opening a small band gap.

## C. Heterostructures MnSe<sub>2</sub>/X (X = GaP, GaSe, SiH, and Al<sub>2</sub>Se<sub>3</sub>)

Considering the mismatch from substrate is an efficient way to provide strain for 2D material in experiments [83], we constructed MnSe<sub>2</sub>-based heterostructures with 2D semiconductors to provide strain. GaP [71, 72], GaSe [74], SiH [75], and Al<sub>2</sub>Se<sub>3</sub> [40] are nonmagnetic semiconductors. The calculated results with PBE at monolayer limit give band gaps of 1.22, 1.80, 2.18 and 1.69 eV, respectively, and lattice constants of 3.916, 3.814, 3.888 and 3.788 Å, respectively. According to the lattice mismatch  $\delta = 2 \times (a_1 - a_2)/(a_1 + a_2) \times 100\%$ , the lattice mismatch of GaP, GaSe, SiH, and Al<sub>2</sub>Se<sub>3</sub> with MnSe<sub>2</sub> are 6.8%, 4.2%, 6.1%, and 3.5%, respectively. The detailed results are given in Supplemental Material [84].

We consider different stacking models of heterostructures, and the detailed data are given in Supplemental Material [84]. As shown in Fig. 4, all heterostructures

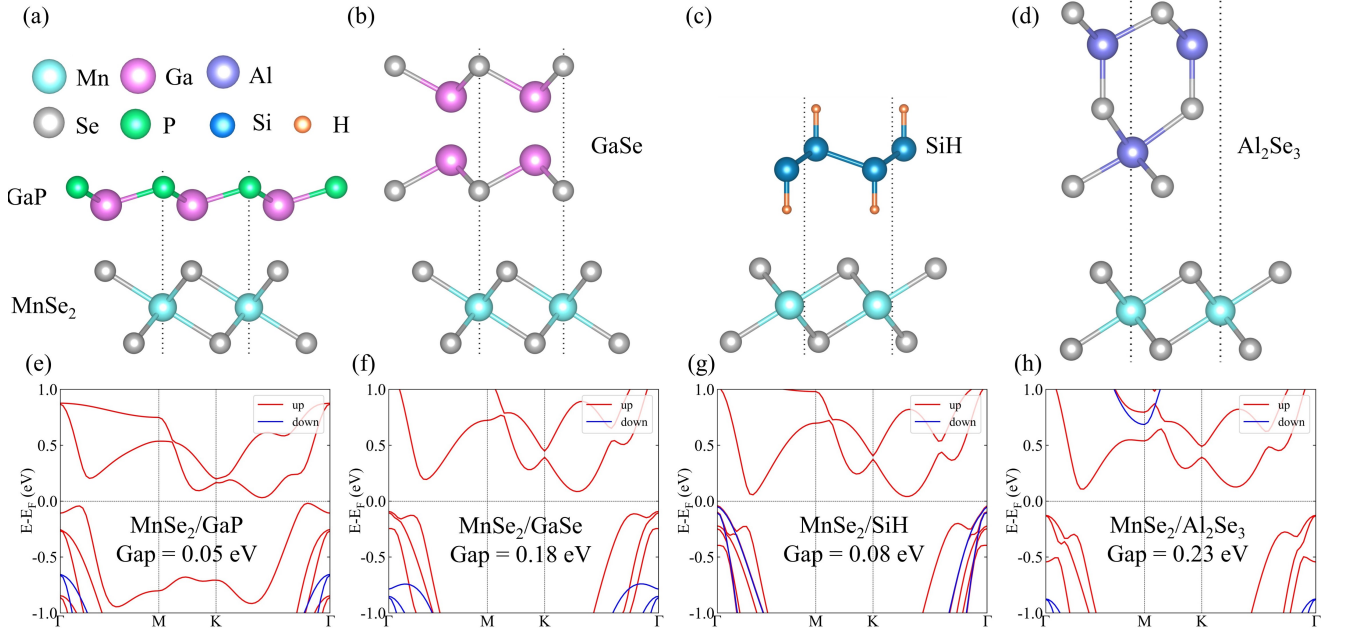


FIG. 4. Structure and spin polarized band structure of  $\text{MnSe}_2$ -based heterostructures, (a, e)  $\text{MnSe}_2/\text{GaP}$ , (b, f)  $\text{MnSe}_2/\text{GaSe}$ , (c, g)  $\text{MnSe}_2/\text{SiH}$ , and (d, h)  $\text{MnSe}_2/\text{Al}_2\text{Se}_3$ . The band structures are obtained by the DFT calculation with HSE hybrid functional.

are ferromagnetic semiconductors. The optimised lattice constants of  $\text{MnSe}_2/\text{X}$  with  $\text{X} = \text{GaP}$ ,  $\text{GaSe}$ ,  $\text{SiH}$ , and  $\text{Al}_2\text{Se}_3$  are about 3.83, 3.76, 3.81, and 3.75 Å, respectively, with an effective tensile strain of 4.7%, 2.8%, 4.2%, and 2.5%, respectively. The binding energy  $E_b$  for  $\text{MnSe}_2/\text{X}$  is defined as  $E_b = (E_{\text{MnSe}_2/\text{X}} - E_{\text{MnSe}_2} - E_{\text{X}})/N_{\text{tot}}$ , where  $E_{\text{MnSe}_2/\text{X}}$ ,  $E_{\text{MnSe}_2}$ , and  $E_{\text{X}}$  represent the total energies of heterostructure  $\text{MnSe}_2/\text{X}$ , monolayer  $\text{MnSe}_2$ , and monolayer  $\text{X}$ , respectively, and  $N_{\text{tot}}$  is the total atom number in a unitcell. The calculated results are -0.24, -0.17, -0.10, and -0.20 eV/atom for  $\text{X} = \text{GaP}$ ,  $\text{GaSe}$ ,  $\text{SiH}$ , and  $\text{Al}_2\text{Se}_3$ , respectively, indicating their stability.  $T_C$  of heterostructures were obtained through DFT calculations and Monte Carlo simulation. As shown in Fig. 2, the calculation results predict that  $\text{MnSe}_2/\text{X}$  with  $\text{X} = \text{GaP}$ ,  $\text{GaSe}$ ,  $\text{SiH}$ , and  $\text{Al}_2\text{Se}_3$  are room temperature magnetic semiconductors with out-of-plane MAE. It is noted that for the heterostructure  $\text{MnSe}_2/\text{GaSe}$ ,  $T_c$  above room temperature and out-of-plane magnetization were observed in the experiment [19]. Thus, our calculation results in Fig. 2 are consistent with the experiment of  $\text{MnSe}_2/\text{GaSe}$  [19]. The detailed calculation results are given in Supplemental Material [84].

Heterostructures not only provide effective strain, but also induce interlayer interaction. The calculated results of the most stable stacks of heterostructures is shown in Fig. 2. The calculated results of heterostructures are different with those of monolayer  $\text{MnSe}_2$  with the same tensile strain. For example, heterostructure  $\text{MnSe}_2/\text{GaSe}$  has a band gap of 0.18 eV, while monolayer  $\text{MnSe}_2$  with same lattice constants has a band gap

of 0.08 eV. Heterostructure  $\text{MnSe}_2/\text{Al}_2\text{Se}_3$  give a MAE of -1.11 meV/Mn, while monolayer  $\text{MnSe}_2$  with same lattice constants give a MAE of -0.36 meV/Mn. Therefore, the interlayer interaction may play an important role in properties of heterostructures.

#### D. MOKE in monolayer $\text{MnSe}_2$ and heterostructures $\text{MnSe}_2/\text{X}$

We investigated the magneto-optical Kerr effect for  $\text{MnSe}_2$  based structures. The Kerr rotation angle is given by:

$$\theta_K(\omega) = \text{Re} \frac{\varepsilon_{xy}}{(1 - \varepsilon_{xx})\sqrt{\varepsilon_{xx}}}, \quad (1)$$

where  $\varepsilon_{xx}$  and  $\varepsilon_{xy}$  are the diagonal and off-diagonal components of the dielectric tensor  $\varepsilon$ , and  $\omega$  is the frequency of incident light. The dielectric tensor  $\varepsilon$  can be obtained by the optical conductivity tensor  $\sigma$  as  $\varepsilon(\omega) = \frac{4\pi i}{\omega} \sigma(\omega) + I$ , where  $I$  is the unit tensor. The calculated Kerr rotation angle as a function of photon energy for monolayer  $\text{MnSe}_2$  with strain is shown in Fig. 5 (a), the result for heterostructures  $\text{MnSe}_2/\text{X}$  with  $\text{X} = \text{GaP}$ ,  $\text{GaSe}$ ,  $\text{SiH}$  and  $\text{Al}_2\text{Se}_3$  is shown in Fig. 5 (b). According to our calculation results, there exist large Kerr rotation angles with out-of-plane magnetization, such as monolayer  $\text{MnSe}_2$  with 2% and 4% tensile strain. On the contrary, Kerr rotation angles with in-plane magnetization are small, such as monolayer  $\text{MnSe}_2$  without strain. In addition, heterostructures  $\text{MnSe}_2/\text{X}$  with out-of-plane magnetization also have a large Kerr rotation angle. The



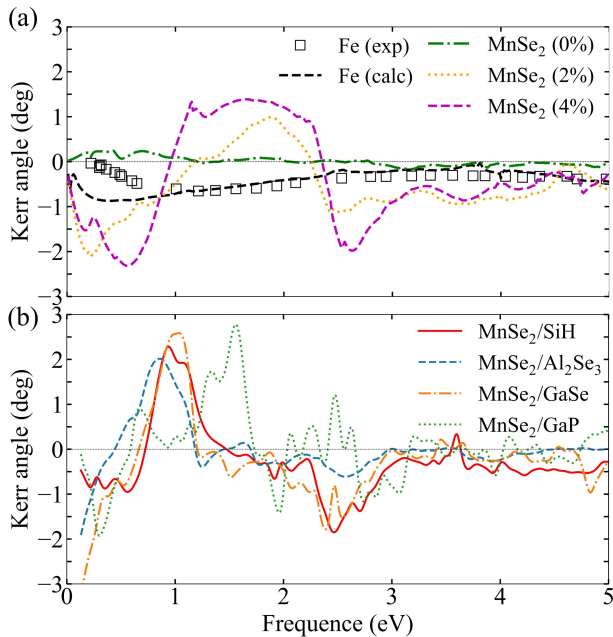


FIG. 5. DFT results of Kerr rotation angle for MnSe<sub>2</sub> with 0%, 2%, 4% tensile strain and heterostructures MnSe<sub>2</sub>/X (X = SiH, Al<sub>2</sub>Se<sub>3</sub>, GaSe, and GaP). Experimental and numerical results of Fe [85] are also included for comparison.

experimental result for Fe [85] and our DFT result for Fe bulk are also included for comparison. The Kerr rotation angles for stretched MnSe<sub>2</sub> are about 4 times bigger than that of bcc Fe. Detailed results of Kerr rotation angles are given in Supplemental Material [84].

## IV. CONCLUSION

Based on the DFT calculations, we studied the properties of monolayer MnSe<sub>2</sub> with strain and MnSe<sub>2</sub>-based heterostructures. For monolayer MnSe<sub>2</sub>, a metal-semiconductor transition happens at 2.2% tensile strain, and an in-plane to out-of-plane MAE transition happens at 1.7% tensile strain. In addition,  $T_C$  of monolayer MnSe<sub>2</sub> increases with tensile strain. The heterostructures MnSe<sub>2</sub>/X with X = GaP, GaSe, SiH, and Al<sub>2</sub>Se<sub>3</sub> were studied, and the DFT calculation results show that they are room temperature ferromagnetic semiconductors with out-of-plane MAE. Large magneto-optical Kerr effect was found in monolayer MnSe<sub>2</sub> with a few percent tensile strain and MnSe<sub>2</sub>-based heterostructures. Our results propose a way to obtain room temperature ferromagnetic semiconductors by metal-semiconductor transition in monolayer MnSe<sub>2</sub> by applying a few percent tensile strain or building heterostructures.

## V. ACKNOWLEDGEMENTS

This work is supported by National Key R&D Program of China (Grant No. 2022YFA1405100), National Natural Science Foundation of China (Grant No. 12074378), Chinese Academy of Sciences (Grants No. YSBR-030, No. JZHKYPT-2021-08, No. XDB33000000), Beijing Municipal Science and Technology Commission (Grant No. Z191100007219013).

- 
- [1] B. Huang, G. Clark, E. Navarro-Moratalla, D. R. Klein, R. Cheng, K. L. Seyler, D. Zhong, E. Schmidgall, M. A. McGuire, D. H. Cobden, W. Yao, D. Xiao, P. Jarillo-Herrero, and X. Xu, Layer-dependent ferromagnetism in a van der Waals crystal down to the monolayer limit, *Nat.* **546**, 270 (2017).
- [2] C. Gong, L. Li, Z. Li, H. Ji, Alex Stern, Y. Xia, T. Cao, W. Bao, C. Wang, Y. Wang, Z. Q. Qiu, R. J. Cava, S. G. Louie, J. Xia, and X. Zhang, Discovery of intrinsic ferromagnetism in two-dimensional van der Waals crystals, *Nat.* **546**, 265 (2017).
- [3] N. D. Mermin and H. Wagner, Absence of Ferromagnetism or Antiferromagnetism in One- or Two-Dimensional Isotropic Heisenberg Models, *Phys. Rev. Lett.* **17**, 1307 (1966).
- [4] J. Chu, Y. Zhang, Y. Wen, R. Qiao, C. Wu, P. He, L. Yin, R. Cheng, F. Wang, Z. Wang, J. Xiong, Y. Li, and J. He, Sub-millimeter-Scale Growth of One-Unit-Cell-Thick Ferrimagnetic Cr<sub>2</sub>S<sub>3</sub> Nanosheets, *Nano. Lett.* **19**, 2154 (2019).
- [5] X. Cai, T. Song, N. P. Wilson, G. Clark, M. He, X. Zhang, T. Taniguchi, K. Watanabe, W. Yao, D. Xiao, M. A. McGuire, D. H. Cobden, and X. Xu, Atomically Thin CrCl<sub>3</sub>: An In-Plane Layered Antiferromagnetic Insulator, *Nano. Lett.* **19**, 3993 (2019).
- [6] Z. Zhang, J. Shang, C. Jiang, A. Rasmita, W. Gao, and T. Yu, Direct Photoluminescence Probing of Ferromagnetism in Monolayer Two-Dimensional CrBr<sub>3</sub>, *Nano. Lett.* **19**, 3138 (2019).
- [7] B. Achinuq, R. Fujita, W. Xia, Y. Guo, P. Bencok, G. van der Laan, and T. Hesjedal, Covalent Mixing in the 2D Ferromagnet CrSiTe<sub>3</sub> Evidenced by Magnetic X-Ray Circular Dichroism, *Phys. Status. Solidi.* **16**, 2100566 (2021).
- [8] K. Lee, A. H. Dismukes, E. J. Telford, R. A. Wiscons, J. Wang, X. Xu, C. Nuckolls, C. R. Dean, X. Roy, and X. Zhu, Magnetic Order and Symmetry in the 2D Semiconductor CrSBr, *Nano. Lett.* **21**, 3511 (2021).
- [9] S. Sun, J. Liang, R. Liu, W. Shen, H. Wu, M. Tian, L. Cao, Y. Yang, Z. Huang, W. Lin, J. Du, Z. Ni, Y. Xu, Q. Chen, and Y. Zhai, Anisotropic magnetoresistance in room temperature ferromagnetic single crystal CrTe flake, *J. Alloy. Compd.* **890**, 161818 (2022).
- [10] L. Meng, Z. Zhou, M. Xu, S. Yang, K. Si, L. Liu, X. Wang, H. Jiang, B. Li, P. Qin, P. Zhang, J. Wang, Z. Liu, P. Tang, Y. Ye, W. Zhou, L. Bao, H.-J. Gao, and Y. Gong, Anomalous thickness dependence of Curie temperature in air-stable two-dimensional ferromagnetic 1T-

- CrTe<sub>2</sub> grown by chemical vapor deposition, *Nat. Commun.* **12**, 94 (2021).
- [11] R. Chua, J. Zhou, X. Yu, W. Yu, J. Gou, R. Zhu, L. Zhang, M. Liu, M. B. H. Breese, W. Chen, K. P. Loh, Y. P. Feng, M. Yang, Y. L. Huang, and A. T. S. Wee, Room Temperature Ferromagnetism of Monolayer Chromium Telluride with Perpendicular Magnetic Anisotropy, *Adv. Mater.* **33**, 2103360 (2021).
- [12] B. Li, X. Deng, W. Shu, X. Cheng, Q. Qian, Z. Wan, B. Zhao, X. Shen, R. Wu, S. Shi, H. Zhang, Z. Zhang, X. Yang, J. Zhang, M. Zhong, Q. Xia, J. Li, Y. Liu, L. Liao, Y. Ye, L. Dai, Y. Peng, B. Li, and X. Duan, Air-stable ultrathin Cr<sub>3</sub>Te<sub>4</sub> nanosheets with thickness-dependent magnetic biskyrms, *Mater. Today* **57**, 66 (2022).
- [13] Y. Zhang, J. Chu, L. Yin, T. Shifa, Z. Cheng, R. Cheng, F. Wang, Y. Wen, X. Zhan, Z. Wang, and J. He, Ultrathin Magnetic 2D Single-Crystal CrSe, *Adv. Mater.* **31**, 1900056 (2019).
- [14] Y. Deng, Y. Yu, Y. Song, J. Zhang, N. Z. Wang, Z. Sun, Y. Yi, Y. Z. Wu, S. Wu, J. Zhu, J. Wang, X. H. Chen, and Y. Zhang, Gate-tunable room-temperature ferromagnetism in two-dimensional Fe<sub>3</sub>GeTe<sub>2</sub>, *Nat.* **563**, 94 (2018).
- [15] Z. Fei, B. Huang, P. Malinowski, W. Wang, T. Song, J. Sanchez, W. Yao, D. Xiao, X. Zhu, A. F. May, W. Wu, D. H. Cobden, J.-H. Chu, and X. Xu, Two-dimensional itinerant ferromagnetism in atomically thin Fe<sub>3</sub>GeTe<sub>2</sub>, *Nat. Mater.* **17**, 778 (2018).
- [16] J. Seo, D. Kim, E. An, K. Kim, G.-Y. Kim, S.-Y. Hwang, D. Kim, B. Jang, H. Kim, G. Eom, S. Seo, R. Stania, M. Muntwiler, J. Lee, K. Watanabe, T. Taniguchi, Y. Jo, J. Lee, B. Min, M. Jo, H. Yeom, S.-Y. Choi, J. Shim, and J. Kim, Nearly room temperature ferromagnetism in a magnetic metal-rich van der Waals metal, *Sci. Adv.* **6**, eaay8912 (2020).
- [17] A. May, D. Ovchinnikov, Q. Zheng, R. Hermann, S. Calder, B. Huang, Z. Fei, Y. Liu, X. Xu, and M. McGuire, Ferromagnetism Near Room Temperature in the Cleavable van der Waals Crystal Fe<sub>5</sub>GeTe<sub>2</sub>, *ACS Nano* **13**, 4436 (2019).
- [18] G. Zhang, F. Guo, H. Wu, X. Wen, L. Yang, W. Jin, W. Zhang, and H. Chang, Above-room-temperature strong intrinsic ferromagnetism in 2D van der Waals Fe<sub>3</sub>GaTe<sub>2</sub> with large perpendicular magnetic anisotropy, *Nat. Commun.* **13**, 5067 (2022).
- [19] D. O'hara, T. Zhu, A. Trout, A. Ahmed, Y. Luo, C. Lee, M. Brenner, S. Rajan, J. Gupta, D. McComb, and R. Kawakami, Room Temperature Intrinsic Ferromagnetism in Epitaxial Manganese Selenide Films in the Monolayer Limit, *Nano. Lett.* **18**, 3125 (2018).
- [20] S. Jiang, L. Li, Z. Wang, K. F. Mak, and J. Shan, Controlling magnetism in 2D CrI<sub>3</sub> by electrostatic doping, *Nat. Nanotechnol.* **13**, 549 (2018).
- [21] J.-Y. You, X.-J. Dong, B. Gu, and G. Su, Electric field induced topological phase transition and large enhancements of spin-orbit coupling and Curie temperature in two-dimensional ferromagnetic semiconductors, *Phys. Rev. B* **103**, 104403 (2021).
- [22] F. Zhao, T. Cao, and S. G. Louie, Topological Phases in Graphene Nanoribbons Tuned by Electric Fields, *Phys. Rev. Lett.* **127**, 166401 (2021).
- [23] J. Shi, Y. Ou, M. A. Migliorato, H. Wang, H. Li, Y. Zhang, Y. Gu, and M. Zou, Tuning the electronic structure of GeC/WS<sub>2</sub> van der Waals heterostructure by electric field and strain: A first principles study, *Comput. Mater. Sci.* **160**, 301 (2019).
- [24] Q. Hao, H. Yi, H. Su, B. Wei, Z. Wang, Z. Lao, Y. Chai, Z. Wang, C. Jin, J. Dai, and W. Zhang, Phase Identification and Strong Second Harmonic Generation in Pure  $\epsilon$ -InSe and Its Alloys, *Nano Lett.* **19**, 2634 (2019).
- [25] B. Wang, Q. Wu, Y. Zhang, Y. Guo, X. Zhang, Q. Zhou, S. Dong, and J. Wang, High Curie-temperature intrinsic ferromagnetism and hole doping-induced half-metallicity in two-dimensional scandium chlorine monolayers, *Nanoscale Horiz.* **3**, 551 (2018).
- [26] S. Feng, Z. Lin, X. Gan, R. Lv, and M. Terrones, Doping two-dimensional materials: ultra-sensitive sensors, band gap tuning and ferromagnetic monolayers, *Nanoscale Horiz.* **2**, 72 (2017).
- [27] J. Fang, H. Song, B. Li, Z. Zhou, J. Yang, B. Lin, Z. Liao, and Z. Wei, Large unsaturated magnetoresistance of 2D magnetic semiconductor Fe-SnS<sub>2</sub> homojunction, *J. Semicond.* **43**, 092501 (2022).
- [28] D. Zhao, C. Zhang, C. Zhang, W. Ji, S. Li, and P. Wang, Magnetic tuning in a novel half-metallic Ir<sub>2</sub>Te<sub>2</sub> monolayer, *J. Semicond.* **43**, 052001 (2022).
- [29] H. González-Herrero, J. M. Gómez-Rodríguez, P. Mallet, M. Moaied, J. J. Palacios, C. Salgado, M. M. Ugeda, J.-Y. Veuillen, F. Yndurain, and I. Brihuela, Atomic-scale control of graphene magnetism by using hydrogen atoms, *Sci.* **352**, 437 (2016).
- [30] S. Datta, Y. Cai, I. Yudhistira, Z. Zeng, Y.-W. Zhang, H. Zhang, S. Adam, J. Wu, and K. P. Loh, Tuning magnetoresistance in molybdenum disulphide and graphene using a molecular spin transition, *Nat. Commun.* **8**, 94 (2017).
- [31] V. Pathirage, S. Khatun, S. Lisenkov, K. Lasek, J. Li, S. Kolekar, M. Valvidares, P. Gargiani, Y. Xin, I. Ponomareva, and M. Batzill, 2D materials by Design: Intercalation of Cr or Mn between two VSe<sub>2</sub> van der Waals Layers, *Nano Lett.* , e2004557 (2023).
- [32] J. Zhou, Z. Lin, H. Ren, X. Duan, I. Shakir, Y. Huang, and X. Duan, Layered Intercalation Materials, *Adv. Mater.* **33**, 9579 (2021).
- [33] W. Chen, Z. Sun, Z. Wang, L. Gu, X. Xu, S. Wu, and C. Gao, Direct observation of van der Waals stacking-dependent interlayer magnetism, *Sci.* **366**, 983 (2019).
- [34] X. Zhang, Q. Lu, W. Liu, W. Niu, J. Sun, J. CoOk, M. Vaninger, P. F. Miceli, D. J. Singh, S.-W. Lian, T.-R. Chang, X. He, J. Du, L. He, R. Zhang, G. Bian, and Y. Xu, Room-temperature intrinsic ferromagnetism in epitaxial CrTe<sub>2</sub> ultrathin films, *Nat. Commun.* **12**, 2492 (2021).
- [35] P. Kumar, Y. S. Chauhan, A. Agarwal, and S. Bhowmick, Thickness and Stacking Dependent Polarizability and Dielectric Constant of Graphene-Hexagonal Boron Nitride Composite Stacks, *J. Phys. Chem. C* **120**, 17620 (2016).
- [36] Z. Chen, X. Liu, X. Li, P. Gao, Z. Li, W. Zhu, H. Wang, and X. Li, Large tunneling magnetoresistance in spin-filtering 1T-MnSe<sub>2</sub>/h-BN van der Waals magnetic tunnel junction, *Nanoscale* **15**, 8447 (2023).
- [37] B. Wu, J. Yang, S. Liu, S. Fang, Z. Liu, Z. Lin, J. Shi, W. Yang, Z. Luo, C. Wang, H. Du, J. Yang, and J. Lu, Layer-Dependent Magnetoresistance and Spin-Transfer Torque in MnSe<sub>2</sub>-Based Magnetic Tunnel Junctions, *Phys. Rev. Applied* **19**, 064008 (2023).

- [38] X.-J. Dong, J.-Y. You, Z. Zhang, B. Gu, and G. Su, Great enhancement of Curie temperature and magnetic anisotropy in two-dimensional van der Waals magnetic semiconductor heterostructures, *Phys. Rev. B* **102**, 144443 (2020).
- [39] S. Chen, C. Huang, H. Sun, J. Ding, P. Jena, and E. Kan, Boosting the Curie Temperature of Two-Dimensional Semiconducting CrI<sub>3</sub> Monolayer through van der Waals Heterostructures, *J. Phys. Chem. C* **123**, 17987 (2019).
- [40] Y. Li, J. Deng, Y.-F. Zhang, X. Jin, W.-H. Dong, J.-T. Sun, J. Pan, and S. Du, Nonvolatile electrical control of spin polarization in the 2D bipolar magnetic semiconductor VSeF, *npj Comput. Mater.* **9**, 50 (2023).
- [41] M. Ren, M. Li, C. Zhang, M. Yuan, P. Li, F. Li, W. Ji, and X. Chen, Band structures in silicene on monolayer gallium phosphide substrate, *Solid State Commun.* **239**, 32 (2016).
- [42] R. Caglayan, H. E. Guler, and Y. Mogulkoc, An analysis of Schottky barrier in silicene/Ga<sub>2</sub>SeS heterostructures by employing electric field and strain, *Phys. Chem. Chem. Phys.* **24**, 10210 (2022).
- [43] G. Yuan, Z. Cheng, Y. Cheng, W. Duan, H. Lv, Z. Liu, C. Han, and X. Ma, Highly Sensitive Band Alignment of the Graphene/MoSi<sub>2</sub>N<sub>4</sub> Heterojunction via an External Electric Field, *ACS Appl. Electron. Mater.* **4**, 2897 (2022).
- [44] J. Yuan, F. Wang, Z. Zhang, B. Song, S. Yan, M.-H. Shang, C. Tong, and J. Zhou, Effects of electric field and interlayer coupling on Schottky barrier of germanene/MoSSe vertical heterojunction, *Phys. Rev. B* **108**, 125404 (2023).
- [45] J. Hong, C.-J. Kang, and J. Kim, Role of electronic correlations in room-temperature ferromagnetism of monolayer MnSe<sub>2</sub>, *Phys. Rev. B* **106**, 195428 (2022).
- [46] J. Yang, X. Wang, S. Li, X. Wang, M. Pan, M. Ai, H. Yuan, X. Peng, R. Wang, Q. Li, F. Zheng, and P. Zhang, Robust Two-Dimensional Ferromagnetism in Cr<sub>5</sub>Te<sub>8</sub>/CrTe<sub>2</sub> Heterostructure with Curie Temperature above 400 K, *ACS Nano*, 23160 (2023).
- [47] W. Zhu, C. Song, L. Han, H. Bai, C. Chen, and F. Pan, Interface-enhanced room-temperature Curie temperature in CrPS<sub>4</sub>/graphene van der Waals heterostructure, *Phys. Rev. B* **108**, 1100406 (2023).
- [48] X. Lu, Y. Deng, Y. Pei, Z. Chen, and G. Wang, Recent advances in NiO/Ga<sub>2</sub>O<sub>3</sub> heterojunctions for power electronics, *J. Semicond.* **44**, 061802 (2023).
- [49] S. Huang, G. Zhang, F. Fan, C. Song, F. Wang, Q. Xing, C. Wang, H. Wu, and H. Yan, Strain-tunable van der Waals interactions in few-layer black phosphorus, *Nat. Commun.* **10**, 94 (2019).
- [50] Z. Li, Y. Lv, L. Ren, J. Li, L. Kong, Y. Zeng, Q. Tao, R. Wu, H. Ma, B. Zhao, D. Wang, W. Dang, K. Chen, L. Liao, X. Duan, X. Duan, and Y. Liu, Efficient strain modulation of 2D materials via polymer encapsulation, *Nat. Commun.* **11**, 94 (2020).
- [51] Z. Xu and H. Zhu, Two-Dimensional Manganese Nitride Monolayer with Room Temperature Rigid Ferromagnetism under Strain, *J. Phys. Chem. C* **122**, 14918 (2018).
- [52] Z. Wu, J. Yu, and S. Yuan, Strain-tunable magnetic and electronic properties of monolayer CrI<sub>3</sub>, *Phys. Chem. Chem. Phys.* **21**, 7750 (2019).
- [53] D. Wei, The room temperature ferromagnetism in highly strained two-dimensional magnetic semiconductors, *J. Semicond.* **44**, 040401 (2023).
- [54] S. Bertolazzi, J. Brivio, and A. Kis, Stretching and Breaking of Ultrathin MoS<sub>2</sub>, *ACS Nano* **5**, 9703 (2011).
- [55] R. Peng, H. C. Xu, S. Y. Tan, H. Y. Cao, M. Xia, X. P. Shen, Z. C. Huang, C. Wen, Q. Song, T. Zhang, B. P. Xie, X. G. Gong, and D. L. Feng, Tuning the band structure and superconductivity in single-layer FeSe by interface engineering, *Nat. Commun.* **5**, 94 (2014).
- [56] P. Zhang, X.-L. Peng, T. Qian, P. Richard, X. Shi, J.-Z. Ma, B. B. Fu, Y.-L. Guo, Z. Q. Han, S. C. Wang, L. L. Wang, Q.-K. Xue, J. P. Hu, Y.-J. Sun, and H. Ding, Observation of high-T<sub>C</sub> superconductivity in rectangular FeSe/SrTiO<sub>3</sub>(110) monolayers, *Phys. Rev. B* **94**, 104510 (2016).
- [57] G. Cocco, E. Cadelano, and L. Colombo, Gap opening in graphene by shear strain, *Phys. Rev. B* **81**, 241412 (2010).
- [58] M. Idrees, M. Khurami, B. Amin, Y. Chen, and X. Yan, Interfacial characteristics, metal-semiconductor contact and optical properties of CSe and BX (X=B, As and Sb) monolayers, *Mat. Sci. Semicon. Proc.* **163**, 107593 (2023).
- [59] H. Hu and G. Ouyang, First-principles calculations of interface engineering for 2D *alpha*-In<sub>2</sub>Se<sub>3</sub>-based van der Waals multiferroic heterojunctions, *Appl. Surf. Sci.* **545**, 149024 (2021).
- [60] B. A. Noesges, T. Zhu, J. J. Repicky, S. Yu, F. Yang, J. A. Gupta, R. K. Kawakami, and L. J. Brillson, Chemical migration and dipole formation at van der Waals interfaces between magnetic transition metal chalcogenides and topological insulators, *Phys. Rev. Materials* **4**, 054001 (2020).
- [61] C. Xiao, W. Wu, H. Wang, Y.-X. Huang, X. Feng, H. Liu, G.-Y. Guo, Q. Niu, and S. A. Yang, Time-Reversal-Even Nonlinear Current Induced Spin Polarization, *Phys. Rev. Lett.* **130**, 166302 (2023).
- [62] I. Eren, F. Iyikanat, and H. Sahin, Defect tolerant and dimension dependent ferromagnetism in MnSe<sub>2</sub>, *Phys. Chem. Chem. Phys.* **21**, 16718 (2019).
- [63] W.-Q. Xie, Z.-W. Lu, C.-C. He, X.-B. Yang, and Y.-J. Zhao, Theoretical study of tunable magnetism of two-dimensional MnSe<sub>2</sub> through strain, charge, and defect, *J. Phys.: Condens. Matter* **33**, 215803 (2021).
- [64] Q. Li, C. xin Zhang, D. Wang, K.-Q. Chen, and L.-M. Tang, Giant valley splitting in a MoTe<sub>2</sub>/MnSe<sub>2</sub> van der Waals heterostructure with room-temperature ferromagnetism, *Mater. Adv.* **3**, 2927 (2022).
- [65] M. Kan, S. Adhikari, and Q. Sun, Ferromagnetism in MnX<sub>2</sub> (X = S, Se) monolayers, *Phys. Chem. Chem. Phys.* **16**, 4990 (2014).
- [66] J. He, S. Li, L. Zhou, and T. Frauenheim, Ultrafast Light-Induced Ferromagnetic State in Transition Metal Dichalcogenides Monolayers, *J. Phys. Chem. Lett.* **13**, 2765 (2022).
- [67] J. Heyd, G. E. Scuseria, and M. Ernzerhof, Hybrid functionals based on a screened Coulomb potential, *J. Chem. Phys.* **118**, 8207 (2003).
- [68] X.-J. Dong, J.-Y. You, B. Gu, and G. Su, Strain-Induced Room-Temperature Ferromagnetic Semiconductors with Large Anomalous Hall Conductivity in Two-Dimensional Cr<sub>2</sub>Ge<sub>2</sub>Se<sub>6</sub>, *Phys. Rev. Appl.* **12**, 014020 (2019).
- [69] Z. Zhang, J.-Y. You, X.-Y. Ma, B. Gu, and G. Su, Kagome quantum anomalous Hall effect with high Chern number and large band gap, *Phys. Rev. B* **103**, 014410 (2021).

- (2021).
- [70] A. O'Neill, S. Rahman, Z. Zhang, P. Schoenherr, T. Yildirim, B. Gu, G. Su, Y. Lu, and J. Seidel, Enhanced Room Temperature Ferromagnetism in Highly Strained 2D Semiconductor  $\text{Cr}_2\text{Ge}_2\text{Te}_6$ , *ACS Nano* **17**, 735 (2022).
- [71] H. Li, Y. Liu, Z. Bai, J. Xiong, F. Liu, G. Zhou, T. Qing, S. Zhang, and J. Lu, Ohmic contact in graphene and hexagonal III-V monolayer (GaP, GaAs, InP, and InAs) van der Waals heterostructures: Role of electric field, *Phys. Lett. A* **433**, 128029 (2022).
- [72] P. Parmar, S. Khengar, and P. Thakor, Structural And Electronic Properties of  $\text{PtSe}_2/\text{GaP}$  Heterostructure, *Mater. Today: Proc.* **67**, 161 (2022).
- [73] T. Wei, X. Li, Z. Li, W. Yang, Y. Wu, Z. Xing, and S. Lu, Interfacial dynamics of  $\text{GaP}/\text{Si}(100)$  heterostructure grown by molecular beam epitaxy, *J. Semicond.* **43**, 122101 (2022).
- [74] W. Li, X. Zhang, J. Yang, S. Zhou, C. Song, P. Cheng, Y.-Q. Zhang, B. Feng, Z. Wang, Y. Lu, K. Wu, and L. Chen, Emergence of ferroelectricity in a nonferroelectric monolayer, *Nat. Commun.* **14**, 2757 (2023).
- [75] A. F. Wani, B. Rani, S. Dhiman, U. B. Sharopov, and K. Kaur, Sih monolayer: A promising two-dimensional thermoelectric material, *Int. J. Energ. Res.* **46**, 10885 (2022).
- [76] G. Kresse and J. Furthmüller, Efficient iterative schemes for ab initio total-energy calculations using a plane-wave basis set, *Phys. Rev. B* **54**, 11169 (1996).
- [77] J. P. Perdew, K. Burke, and M. Ernzerhof, Generalized Gradient Approximation Made Simple, *Phys. Rev. Lett.* **77**, 3865 (1996).
- [78] P. E. Blöchl, Projector augmented-wave method, *Phys. Rev. B* **50**, 17953 (1994).
- [79] S. Grimme, J. Antony, S. Ehrlich, and H. Krieg, A consistent and accurate ab initio parametrization of density functional dispersion correction DFT-D for the 94 elements H-Pu, *J. Chem. Phys.* **132**, 154104 (2010).
- [80] A. A. Mostofi, J. R. Yates, Y.-S. Lee, I. Souza, D. Vanderbilt, and Nicola Marzari, wannier90: A tool for obtaining maximally-localised Wannier functions, *Comput. Phys. Commun.* **178**, 685 (2008).
- [81] A. A. Mostofi, J. R. Yates, G. Pizzi, Y.-S. Lee, I. Souza, D. Vanderbilt, and Nicola Marzari, An updated version of wannier90: A tool for obtaining maximally-localised wannier functions, *Comput. Phys. Commun.* **185**, 2309 (2014).
- [82] Q. Wu, S. Zhang, H.-F. Song, M. Troyer, and Alexey A. Soluyanov, Wanniertools: An open-source software package for novel topological materials, *Comput. Phys. Commun.* **224**, 405 (2018).
- [83] Y. Qi, M. A. Sadi, D. Hu, M. Zheng, Z. Wu, Y. Jiang, and Y. P. Chen, Recent Progress in Strain Engineering on Van der Waals 2D Materials: Tunable Electrical, Electrochemical, Magnetic, and Optical Properties, *Adv. Mater.* **35**, 2205714 (2023).
- [84] See supplemental material.
- [85] P. M. Oppeneer, T. Maurer, J. Sticht, and J. Kübler, Ab initio calculated magneto-optical Kerr effect of ferromagnetic metals: Fe and Ni, *Phys. Rev. B* **45**, 10924 (1992).